

## Nano-structuring of all-d-metal NiCoMnTi-based Heusler compounds

Zhang, Fengqi; van Dijk, Niels; Brück, Ekkes; Ren, Yang

**DOI**

[10.1063/5.0203383](https://doi.org/10.1063/5.0203383)

**Publication date**

2024

**Document Version**

Final published version

**Published in**

Applied Physics Letters

**Citation (APA)**

Zhang, F., van Dijk, N., Brück, E., & Ren, Y. (2024). Nano-structuring of all-d-metal NiCoMnTi-based Heusler compounds. *Applied Physics Letters*, 124(18), Article 182407. <https://doi.org/10.1063/5.0203383>

**Important note**

To cite this publication, please use the final published version (if applicable). Please check the document version above.

**Copyright**

Other than for strictly personal use, it is not permitted to download, forward or distribute the text or part of it, without the consent of the author(s) and/or copyright holder(s), unless the work is under an open content license such as Creative Commons.

**Takedown policy**

Please contact us and provide details if you believe this document breaches copyrights. We will remove access to the work immediately and investigate your claim.

RESEARCH ARTICLE | MAY 02 2024

# Nano-structuring of all-d-metal NiCoMnTi-based Heusler compounds

Fengqi Zhang   ; Niels van Dijk  ; Ekkes Brück  ; Yang Ren  

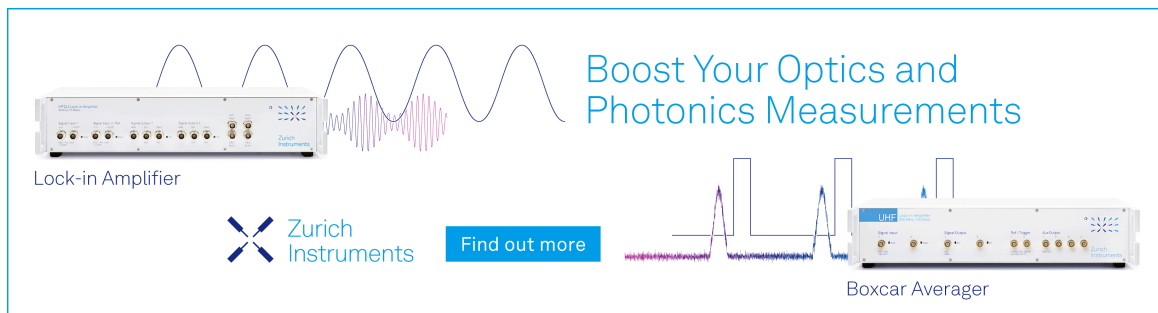
 Check for updates

*Appl. Phys. Lett.* 124, 182407 (2024)


<https://doi.org/10.1063/5.0203383>



Boost Your Optics and Photonics Measurements



Lock-in Amplifier



Find out more

Boxcar Averager

# Nano-structuring of all-*d*-metal NiCoMnTi-based Heusler compounds

Cite as: Appl. Phys. Lett. **124**, 182407 (2024); doi: [10.1063/5.0203383](https://doi.org/10.1063/5.0203383)

Submitted: 13 February 2024 · Accepted: 24 April 2024 ·

Published Online: 2 May 2024



View Online



Export Citation



CrossMark

Fengqi Zhang,<sup>1,2,a)</sup>  Niels van Dijk,<sup>2</sup>  Ekkes Brück,<sup>2</sup>  and Yang Ren<sup>1,a)</sup> 

## AFFILIATIONS

<sup>1</sup>Department of Physics, City University of Hong Kong, Kowloon, Hong Kong

<sup>2</sup>Fundamental Aspects of Materials and Energy (FAME), Faculty of Applied Sciences, Delft University of Technology, Mekelweg 15, 2629JB Delft, The Netherlands

<sup>a)</sup>Authors to whom correspondence should be addressed: [F.Zhang-7@tudelft.nl](mailto:F.Zhang-7@tudelft.nl) and [yangren@cityu.edu.hk](mailto:yangren@cityu.edu.hk)

## ABSTRACT

The emerging all-*d*-metal Ni(Co)MnTi-based Heusler compounds attract extensive attention because it can potentially be employed for solid-state refrigeration. However, in comparison to the abundant physical functionalities in bulk conditions, the hidden properties related to the NiCoMnTi-based Heusler nanoparticles (NPs) have not yet been investigated experimentally. Here, we present NiCoMnTi Heusler NPs that have been manufactured by spark ablation under Ar gas flow, and the related magnetic and microstructural properties have been studied. Compared with the bulk sample, it is found that the magneto-structurally coupled transition in the bulk sample has collapsed into a magnetic transition for the NPs sample. Superparamagnetic NPs with widely distributed dislocations have directly been observed by high-resolution transmission electron microscopy. For the NPs, the magnetocrystalline anisotropy constant is  $3.54 \times 10^4$  J/m<sup>3</sup>, while the saturation magnetization after post-treatment has been estimated to be around 26 Am<sup>2</sup> kg<sup>-1</sup>. Our current research reveals that Ni-Co-Mn-Ti-based quaternary NPs could show interesting properties for future nano-application, and the produced NPs will further expand the functionalities of this material family.

Published under an exclusive license by AIP Publishing. <https://doi.org/10.1063/5.0203383>

Giant magnetocaloric effect materials (GMCMs) generally correspond to magnetic materials that show a first-order magnetic transition (FOMT) from a disordered to an ordered magnetic state.<sup>1</sup> Using these functional materials, specific emerging eco-sustainable applications can be designed, like solid-state magnetic refrigeration,<sup>2–4</sup> magnetic heat pumps,<sup>5</sup> and thermomagnetic generators.<sup>6,7</sup> Several model GMCMs have been found, including Gd<sub>5</sub>(Si<sub>2</sub>Ge<sub>2</sub>),<sup>1</sup> (Mn,Fe)<sub>2</sub>(P,X)-based compounds (X = As, Ge, and Si),<sup>8</sup> La(Fe,Si)<sub>13</sub>-based materials,<sup>9</sup> NiMn-X-based magnetic Heusler alloys (X = Al, Ga, In, Sn, and Sb).<sup>10</sup> Recently, a new family of giant magnetocaloric effect (GMCE) materials named all-*d*-metal Ni(Co)MnTi-based Heusler compounds have received significant attention due to their unique *d-d* hybridization bonding properties,<sup>11</sup> well-tunable GMCE,<sup>12–15</sup> and good mechanical properties,<sup>16,17</sup> compared with traditional NiMn-based magnetic Heusler compounds. Considerable efforts have been spent to investigate the bulk physical functionalities, such as solid-state caloric effects,<sup>11,18,19</sup> high-temperature shape memory effect,<sup>20</sup> giant exchange bias,<sup>21</sup> magnetoresistance,<sup>22</sup> and thermal energy storage applications.<sup>23</sup> However, the potential for fruitful functionalities at nanoscale have not yet been investigated, which necessitates the present study.

For the nanoscale magnetocaloric materials (MCMs), some devices have been proposed and developed in fields like micro-refrigerators,<sup>24,25</sup> microfluidic pumps,<sup>26,27</sup> thermal switches,<sup>28</sup> energy-harvesting devices,<sup>29</sup> frequency-dependent resonators/transducers,<sup>30</sup> and biomedical applications (e.g., magnetic hyperthermia<sup>31</sup> or drug delivery<sup>32</sup>). In comparison to bulk materials, nano-sized particles have several distinct properties, like a high surface-to-volume ratio and a fast thermal response. Several “top-down” and “bottom-up” methods have been applied to control the dimensions of the GMCMs at nanoscale. On the one hand, the high-energy mechanical milling method can significantly reduce the crystalline size of materials from  $\mu\text{m}$  to nm, as, e.g., observed in traditional Ni-Mn-Ga<sup>30,33</sup> and Ni-Mn-In<sup>34,35</sup> Heusler compounds and in (Mn,Fe)<sub>2</sub>(P,Si) materials.<sup>36</sup> By applying the high-energy ball milling technique, Zhang *et al.* observed a crystalline core and an atomically disordered shell-type nanostructure in (Mn, Fe)<sub>2</sub>(P,Si)-based nano MCMs.<sup>36</sup> Different from the above top-down way, the bottom-up methods, such as sol-gel chemistry synthesis, can generally produce nano-structures with a more homogeneous size distribution. For the Heusler compounds at nanoscale, progress has been achieved with the sol-gel method in different compositions, such as

$\text{Co}_2\text{FeSn}$ ,<sup>37</sup>  $\text{Ni}_2\text{FeGa}$ ,<sup>38</sup>  $\text{Fe}_3\text{Ga}$ ,<sup>39</sup>  $\text{Co}_2\text{FeAl}$ ,<sup>40</sup>  $\text{Co}_2\text{FeGa}$ ,<sup>41–43</sup> and  $\text{Co}_2\text{NiGa}$ .<sup>44</sup> Nonetheless, for compositions that contain Mn, the strong tendency toward oxidization of Mn during the sol-gel reaction is limiting to obtain the pure Heusler phase,<sup>42</sup> and multi-step procedures are always time consuming. In contrast, the spark ablation technique can be utilized to produce high-purity nanoparticles (NPs) in a continuous fashion, and the particle properties can easily be optimized by tuning the parameters of the spark ablation device (e.g., current, voltage, and carrier gas speed).<sup>45–47</sup> Recently, the spark ablation technique has been applied to produce NPs with sizes ranging from atomic clusters up to 20 nm.<sup>47</sup> For instance, Feng *et al.* reported the study of the magnetic properties in spark-produced  $\text{La}(\text{Fe},\text{Si})_{13}$ -based MCMs NPs, which show a good magnetic response, such as a high magnetization and maintaining the magnetic phase transition.<sup>45</sup> This technique demonstrates its potentials to further unlock the functionalities for the new all-*d*-metal  $\text{Ni}(\text{Co})\text{MnTi}$  Heusler compounds at nanoscale.

In the present study, using spark ablation equipped with self-designed electrodes (suction-cast  $\text{Ni}_{37}\text{Co}_{13}\text{Mn}_{35}\text{Ti}_{15}$  compounds<sup>15</sup>), the corresponding Ni-Co-Mn-Ti-based NPs have been produced, and the magnetic and microstructural properties are reported. In comparison with the bulk sample, it was found that the magneto-structurally coupled transition transformed into a magnetic transition in the sparked NPs. The superparamagnetic (SPM) NPs show widely distributed lattice dislocations, as revealed by high-resolution transmission electron microscopy (HRTEM). The magnetocrystalline anisotropy and the saturation magnetization associated with the NPs have been studied. Our current research indicates that the Ni-Co-Mn-Ti-based quaternary NPs could show promising properties for future nano-application scenarios like ferro-fluids<sup>48,49</sup> and heterogeneous catalysis.<sup>50</sup>

High-purity (99.9%) raw materials are used to prepare polycrystalline samples with a nominal composition of  $\text{Ni}_{37}\text{Co}_{13}\text{Mn}_{35}\text{Ti}_{15}$  using arc-melting, followed with suction casting under an Ar atmosphere. The applied synthesis process has been reported in our previous paper.<sup>15</sup> After the heat treatment, the suction-cast (SC) bulk samples were rapidly quenched in cold water (named “SC bulk”). Subsequently, the corresponding quaternary Ni-Co-Mn-Ti NPs were synthesized using the spark ablation technique, using a commercial setup (model VSP-G1).<sup>47</sup> A pair of cylindrical  $\text{Ni}_{37}\text{Co}_{13}\text{Mn}_{35}\text{Ti}_{15}$  electrodes (with a diameter of 8 mm and a length of 30 mm) was placed in the generator, where the electrodes face each other at a gap distance of about 10 mm in a carrier gas flow (99.996% Ar) oriented perpendicular to the electrodes. Pulsed sparks were produced in the gap between these two electrodes after applying a high voltage. Consequently, the

generated NPs were collected on a membrane filter at the end of the chamber (NPs). A post-treatment is applied at 400 °C under a  $\text{N}_2$  atmosphere (NPs 400 °C) for 1 h. X-ray diffraction (XRD) patterns of the NPs were collected at room temperature using a PANalytical X-pert Pro diffractometer with  $\text{Cu } K_\alpha$  radiation. The temperature-dependent magnetization ( $M-T$ ) and the field-dependent magnetization ( $M-H$ ) curves for all samples were measured using a superconducting quantum interference device (SQUID, Quantum Design MPMS 5XL) magnetometer. HRTEM images, scanning transmission electron microscopy (STEM) images, and electron energy loss spectroscopy (EELS) maps were obtained using a 300 kV aberration-corrected (S) TEM (JEM-ARM300F, JEOL Ltd) operated at 300 kV with a cold field-emission gun and double dodeca-pole spherical aberration correctors. The TEM analysis was performed using the DigitalMicrograph software (GMS 3, Gatan Inc).

Figure 1(a) shows the self-designed electrodes based on the Ni-Co-Mn-Ti quaternary compounds that were utilized to generate the corresponding NPs. In Fig. 1(b), the  $M-T$  curves in an applied field of 1 T show that the magnetization of the SC NPs sample markedly dropped in comparison with the corresponding bulk compound. The sharp FOMT characteristic of the bulk sample has collapsed for the NPs. It is found that the post-treatment (1 h at 400 °C in  $\text{N}_2$  atmosphere) can slightly recover the magnetization from 10.9 to 12.7  $\text{Am}^2\text{kg}^{-1}$  for the NPs 400 °C sample. The exchange length, which is the length scale over which the direction of magnetization of a ferromagnet can adapt to dipolar fields, generally ranges only from 2 to 5 nm.<sup>51</sup> Thus, in comparison to its bulk counterpart, the significant reduction in magnetization of the Ni-Co-Mn-Ti NPs could result from the reduced exchange interaction among the magnetic atoms. A strong correlation between a reduced crystal size and a significant reduction in saturation magnetization has also been observed in  $(\text{Mn},\text{Fe})_2(\text{P},\text{Si})$  nano MCMs.<sup>36</sup> Additionally, using zero-field cooled (ZFC) and field cooled (FC) magnetization vs temperature measurements, the blocking temperature ( $T_b$ ), which is a key feature for SPM particles, and the individual nanoparticle will become a single magnetic domain and present SPM behavior when the temperature is above this temperature;<sup>52</sup> this can be determined from the peak of ZFC magnetization. The ZFC process is achieved by cooling the sample under zero field, applying the field at 5 K, and then measuring the magnetization with constant field and temperature increase. The ZFC curve peaks at a temperature associated with a typical scale of the anisotropy energy barriers in the NPs system, and this temperature (also refers to  $T_b$ ) stands for that the magnetic anisotropy barriers of NPs are overcome by the thermal

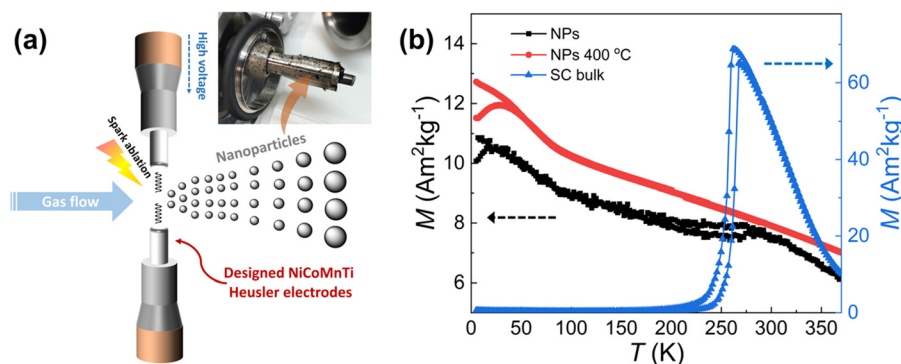


**FIG. 1.** (a) Experimental scheme for the spark-ablation technique. The inset presents residual NPs on the surface of the electrodes after sparking. (b) Iso-field  $M-T$  curves for the NPs, the NPs 400 °C, and the corresponding SC bulk samples in an applied magnetic field of 1 T.

activation and the whole system becomes SPM.<sup>53,54</sup> The obtained value of  $T_b$  (at 1 T) is about 19 and 31 K for the NPs and the NPs 400 °C, respectively. It is found that post annealing at a medium temperature causes a slight increase in  $T_b$ .

As shown in Fig. 2(a), the microstructure and morphology of the Ni-Co-Mn-Ti SPM NPs are probed by HRTEM. The aggregation of NPs is observed, as well as for the NPs 400 °C sample [shown in Fig. S1(a) in the supplementary material]. This happens because there is no surface functionalization for the formation of these NPs.<sup>55</sup> For smaller NPs, the attachment efficiency will be higher as the smaller particles aggregate more readily than larger particles.<sup>56</sup> In Fig. 2(b) and Fig. S1(b) (supplementary material), the average grain sizes are estimated as 7.7 and 9.4 nm for the NPs and the NPs 400 °C samples, respectively. The nanoscale dimension (below 10 nm) further supports the SPM behavior of these NPs. The corresponding fast Fourier transform (FFT) pattern in Fig. 2(c) is consistent with the austenitic cubic lattice structure ( $Fm-3m$ , space group 225), which is in agreement with the XRD results, as shown in Fig. S2. In comparison to the SC bulk sample, the XRD pattern of NPs sample shows an obvious broadening due to a significant reduction in grain size. In Fig. 2(d), an abundant amount of lattice dislocations is found from the inverse fast Fourier transform (IFFT) pattern. In Fig. 2(e), examples of edge dislocations are directly observable in the high-resolution lattice image; the interplanar spacing  $d$  for the (220) reflection is about 0.21 nm. It is known that a high density of dislocations can result in a pinning force for the motion

of the magnetic domain walls.<sup>57</sup> However, as presented in Fig. S1(d) (supplementary material), the post-treatment (NPs 400 °C) can efficiently eliminate these dislocations. This explains the thermal hysteresis for the SC NPs sample observed in Fig. 1(b) (the heating and cooling curves do not coincide at 250 K). To probe the martensitic transformation (MT), an XRD pattern for the NPs sample is also collected at 200 K. As shown in Fig. S2, it is found that only the austenite phase is present at low temperatures, which indicates that the MT is suppressed and the transition is isostructural for these NPs (grain size  $\sim 7.7$  nm). It has been found earlier that the grain size can significantly influence the behavior of MT. For example, for the Heusler alloys, NiMnSn and NiMnGa, the critical grain sizes for the MT are around 9 and 16 nm, respectively.<sup>58,59</sup> In another words, when the grain size is below a critical value, the martensite-to-austenite transition will be suppressed and only a magnetic transition will survive. Moreover, in nanocrystalline NiTi alloys, the MT was completely suppressed for grain sizes smaller than 60 nm.<sup>60</sup> The reason could be that with decreasing grain size and decreasing twin separation, which is a prerequisite for martensite nucleation, both the strain energy and the twin interfacial energy will cause an increasing energy barrier for the MT.<sup>60,61</sup> The selected area electron diffraction (SAED) pattern for an individual NP shown in Fig. 2(f) confirms the cubic structure. As shown in Figs. 2(h)–2(k) and Figs. S1(f)–S1(i) (supplementary material), the different elemental EELS maps show a homogeneous distribution for both the NPs and the NPs 400 °C samples. Additionally, electron energy loss spectra

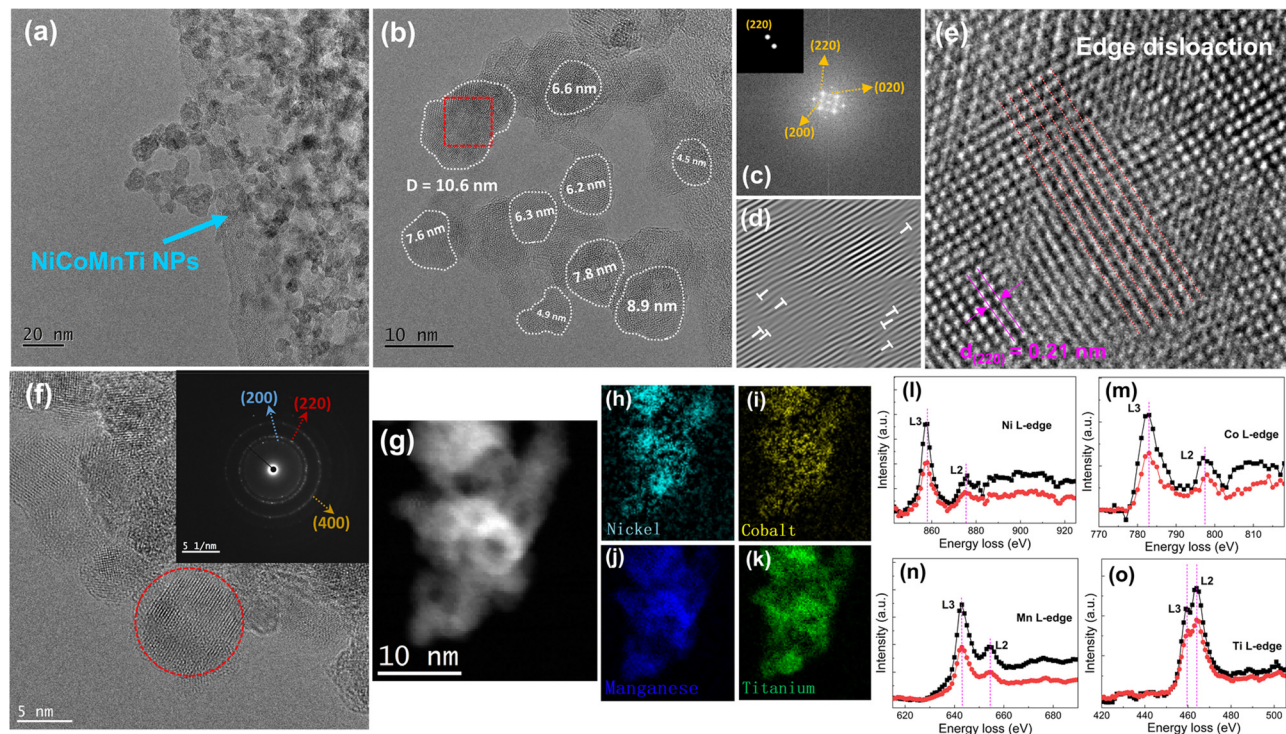


**FIG. 2.** (a) HRTEM image for the NPs sample. (b) The HRTEM image for separate crystallites distributed within the matrix. The average crystallite diameter is around 7.7 nm. (c) FFT patterns in the regions indicated by the red box in (b). (d) Corresponding IFFT pattern of (c) consisting of numerous dislocations marked with "T" along the [220] direction. (e) Enlarged details of the HRTEM image from the red region in (b). (f) The HRTEM image and the corresponding electron diffraction patterns of the NPs sample. (g) Annular dark-field (ADF) STEM image. (h)–(k) EELS maps for Ni, Co, Mn, and Ti, respectively. (l)–(o) Electron energy loss spectra (L-edge) for Ni, Co, Mn, and Ti for the NPs (black) and the NPs 400 °C (red) samples, respectively.

(*L*-edge) of Ni, Co, Mn, and Ti for the NPs and NPs 400 °C samples are compared and no energy difference is observed. This indicates that there is no modification of the chemical composition before and after the post-treatment. As mentioned before, only a slight increase in particle size was observed after the post-treatment.

For the SPM NPs, the SPM relaxation time ( $\tau$ ) can be described in terms of the Néel-Brown-Arrhenius expression:<sup>62</sup>  $\tau = \tau_0 e^{E_b/k_B T}$ , where  $E_b \cong KV$  is the energy barrier of the system,  $K$  is the magnetic anisotropy constant,  $V$  is the particle volume,  $T$  is the temperature,  $\tau_0$  is the characteristic time constant (generally in the range of  $10^{-12}$ – $10^{-9}$  s), and  $k_B$  is the Boltzmann constant. For conventional magnetometry, like MPMS, the characteristic  $\tau$  is of the order of 100 s.<sup>63,64</sup> Therefore, the magnetic anisotropy constant of Ni-Co-Mn-Ti SPM NPs can be estimated from the modified Néel-Brown-Arrhenius expression by the following equation:

$$K = k_B T \ln(\tau/\tau_0)/V. \quad (1)$$

Because  $T_b$  can be also expressed as  $T_b \sim KV/k_B \ln(\tau_m/\tau_0)$  with a characteristic measurement time of  $\tau_m = 100$  s. When the  $T = T_b$ , for the NPs sample, the magnetic anisotropy constant is estimated to be  $K = 3.54 \times 10^4$  J/m<sup>3</sup>, assuming that the NPs are spherical in shape and uniform in size with  $\tau_0 = 10^{-12}$  s.<sup>42</sup> This value is of the same order of magnitude as the reported magnetic anisotropy of other Heusler NPs like Co<sub>2.0</sub>Fe<sub>1.09</sub>Ga<sub>0.66</sub> ( $K = 1.59 \times 10^4$  J/m<sup>3</sup>).<sup>42</sup>

In Fig. 3(a), the  $M$ - $H$  curves are shown for the NPs samples in the ferromagnetic state at 5 K. The magnetization reaches a maximum value ( $M_{\max}$ ) of about 20 Am<sup>2</sup> kg<sup>-1</sup> K<sup>-1</sup> at the maximum field (5 T) without showing saturation. To further study the magnetic hysteresis of these magnetic NPs the coercive field  $\mu_0 H_c$  is derived from the hysteresis loops for the NPs. As shown in the inset of Fig. 3(a), the value of  $\mu_0 H_c$  amounts to 0.04 T, which means that the NPs correspond to soft magnetic materials. The small hysteresis loss during the magnetization and demagnetization processes could result from the enhanced magnetocrystalline anisotropy at lower temperatures.<sup>65,66</sup> To acquire further information about the magnetic properties of the NPs, the law of approach to saturation (LAS) is applied for the NPs and the NPs 400 °C samples. The LAS model describes the high-field approach to saturation of the magnetization

curve in ferromagnetic materials.<sup>51,67,68</sup> Careful understanding about LAS model can be found in book.<sup>69</sup> For ferromagnetic materials, it is known that in the high-field region, domain rotation is the predominant effect. In this field range, the LAS model is applicable as the changes in  $M$  with field are relatively small.<sup>69</sup> As demonstrated in Fig. 3(b), the  $M$ - $H$  curves of these two samples are fitted by the LAS model as follows:

$$M = M_S \left( 1 - \frac{a}{H} - \frac{b}{H^2} \right) + \chi_{hf} H, \quad (2)$$

where  $M_S$  is the spontaneous magnetization,  $a$  and  $b$  are constants, and  $\chi_{hf}$  is the high-field susceptibility. The term  $a/H$  describes the effect of structural defects or voids in the sample, the term  $b/H^2$  the effect of the magnetocrystalline anisotropy, and the term  $\chi_{hf} H$  the effect of the high-field susceptibility due to a field-induced band splitting.<sup>51,69</sup> In Fig. 3(b), the fit results of the LAS model show a good match with the experimental data for NPs and the NPs 400 °C samples. Based on the fits, the extracted saturation magnetization is around 26 Am<sup>2</sup> kg<sup>-1</sup> for the NPs 400 °C sample.

In summary, quaternary Ni-Co-Mn-Ti-based SPM Heusler NPs (<10 nm) have been produced by utilizing the spark ablation technique (a top-down approach), and their basic magnetic and microstructural properties have been investigated. In comparison with the bulk sample, it is found that the magneto-structurally coupled transition has transformed into an isostructural magnetic transition for the NPs sample. The microstructure of the SPM NPs has been investigated by HRTEM, showing widely distributed dislocations. A post-treatment can efficiently remove these dislocations and slightly recover the magnetization, in comparison with the original NPs. From the EELS results before and after the post-treatment, it is found that the NPs do not show chemical shifts. The corresponding magnetocrystalline anisotropy constant  $K$  of the NPs is estimated at  $3.54 \times 10^4$  J/m<sup>3</sup>, while the saturation magnetization associated with the NPs 400 °C sample is estimated with the LAS model at 26 Am<sup>2</sup> kg<sup>-1</sup>. Our present results indicate that the spark-produced Ni-Co-Mn-Ti-based quaternary NPs show interesting properties for future nano-applications. These SPM NPs will further expand the potential functionalities of this material family.

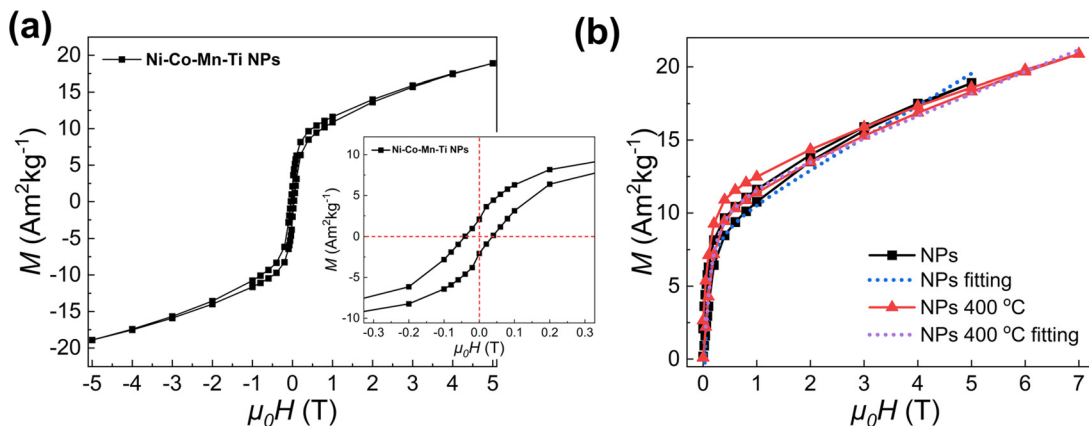


**FIG. 3.** (a) Isothermal  $M$ - $H$  loops (up to 5 T) for the Ni-Co-Mn-Ti NPs at 5 K. The inset shows an enlargement from (a). (b)  $M$ - $H$  curves (up to 7 T) for the NPs and curves (up to 5 T) for the NPs 400 °C at 5 K. The dashed lines are fits using the LAS model.

See the [supplementary material](#) for additional experimental results including high-resolution microscope data for the NPs 400 °C sample and XRD data for NPs sample.

The authors thank Anton Lefering, Bert Zwart, Robert Dankelman, and Michel Steenvoorden for their technical assistance. F. Zhang greatly appreciates the kind help from Dr. Y. K. Huang (Van der Waals-Zeeman Institute, University of Amsterdam) for sample preparation (vacuum suction casting), and Rogier van Oossanen and Dr. Antonia G. Denkova (Applied Radiation & Isotopes, Delft University of Technology) for the NPs production experiments. This work was supported by the open research fund of CNS (Grant Nos. KFKT2022A05 and KFKT2022B04) and the NWO in the domain of the Applied and Engineering Sciences (AES) program. F. Zhang and Y. Ren acknowledge financial support from the City University of Hong Kong (Project No. 9610533).

## AUTHOR DECLARATIONS

### Conflict of Interest

The authors have no conflicts to disclose.

### Author Contributions

**Fengqi Zhang:** Conceptualization (equal); Data curation (equal); Formal analysis (equal); Investigation (equal); Validation (equal); Writing – original draft (equal); Writing – review & editing (equal). **Niels van Dijk:** Formal analysis (equal); Funding acquisition (equal); Supervision (equal); Writing – original draft (equal); Writing – review & editing (equal). **Ekkas Bruck:** Conceptualization (equal); Funding acquisition (equal); Supervision (equal); Writing – original draft (equal); Writing – review & editing (equal). **Yang Ren:** Funding acquisition (equal); Supervision (equal); Writing – original draft (equal); Writing – review & editing (equal).

### DATA AVAILABILITY

The data that support the findings of this study are available from the corresponding authors upon reasonable request.

## REFERENCES

- V. K. Pecharsky and K. A. Gschneidner, Jr., “Giant magnetocaloric effect in  $Gd_5(Si_2Ge_2)$ ,” *Phys. Rev. Lett.* **78**, 4494 (1997).
- V. Franco, J. S. Blazquez, J. J. Ipus, J. Y. Law, L. M. Moreno-Ramirez, and A. Conde, “Magnetocaloric effect: From materials research to refrigeration devices,” *Prog. Mater. Sci.* **93**, 112 (2018).
- A. Kitanovski, “Energy applications of magnetocaloric materials,” *Adv. Energy Mater.* **10**, 1903741 (2020).
- X. Moya and N. D. Mathur, “Caloric materials for cooling and heating,” *Science* **370**, 797 (2020).
- H. Johra, K. Filonenko, P. Heiselberg, C. Veje, S. Dall’Olio, K. Engelbrecht, and C. Bahl, “Integration of a magnetocaloric heat pump in an energy flexible residential building,” *Renewable Energy* **136**, 115 (2019).
- T. Christiaan and E. Brück, “Proof-of-concept static thermomagnetic generator experimental device,” *Metall. Mater. Trans. E* **1**, 36 (2014).
- A. Waske, D. Dzekan, K. Sellschopp, D. Berger, A. Stork, K. Nielsch, and S. Fähler, “Energy harvesting near room temperature using a thermomagnetic generator with a pretzel-like magnetic flux topology,” *Nat. Energy* **4**, 68 (2018).
- O. Tegus, E. Brück, K. H. J. Buschow, and F. R. de Boer, “Transition-metal-based magnetic refrigerants for room-temperature applications,” *Nature* **415**, 150 (2002).
- F. X. Hu, B. G. Shen, J. R. Sun, Z. H. Cheng, G. H. Rao, and X. X. Zhang, “Influence of negative lattice expansion and metamagnetic transition on magnetic entropy change in the compound  $LaFe_{11.4}Si_{1.6}$ ,” *Appl. Phys. Lett.* **78**, 3675 (2001).
- A. Planes, L. Manosa, and M. Acet, “Magnetocaloric effect and its relation to shape-memory properties in ferromagnetic Heusler alloys,” *J. Phys.: Condens. Matter* **21**, 233201 (2009).
- Z. Y. Wei, E. K. Liu, J. H. Chen, Y. Li, G. D. Liu, H. Z. Luo, X. K. Xi, H. W. Zhang, W. H. Wang, and G. H. Wu, “Realization of multifunctional shape-memory ferromagnets in all-*d*-metal Heusler phases,” *Appl. Phys. Lett.* **107**, 022406 (2015).
- H. N. Bez, A. K. Pathak, A. Biswas, N. Zarkevich, V. Balema, Y. Mudryk, D. D. Johnson, and V. K. Pecharsky, “Giant enhancement of the magnetocaloric response in Ni-Co-Mn-Ti by rapid solidification,” *Acta Mater.* **173**, 225 (2019).
- A. Taubel, B. Beckmann, L. Pfeuffer, N. Fortunato, F. Scheibel, S. Ener, T. Gottschall, K. P. Skokov, H. R. Zhang, and O. Gutfleisch, “Tailoring magnetocaloric effect in all-*d*-metal Ni-Co-Mn-Ti Heusler alloys: A combined experimental and theoretical study,” *Acta Mater.* **201**, 425 (2020).
- B. Beckmann, D. Koch, L. Pfeuffer, T. Gottschall, A. Taubel, E. Adabifiroozjiaei, O. N. Miroshkina, S. Riegg, T. Niehoff, N. A. Kani, M. E. Gruner, L. Molina-Luna, K. P. Skokov, and O. Gutfleisch, “Dissipation losses limiting first-order phase transition materials in cryogenic caloric cooling: A case study on all-*d*-metal Ni(-Co)-Mn-Ti Heusler alloys,” *Acta Mater.* **246**, 118695 (2023).
- F. Q. Zhang, Z. Y. Wu, J. L. Wang, W. Y. Chen, Z. D. Wu, X. Chi, C. L. Zhao, S. W. H. Eijt, H. Schut, X. D. Bai, Y. Ren, N. van Dijk, and E. Brück, “Impact of fast-solidification on all-*d*-metal NiCoMnTi based giant magnetocaloric Heusler compounds,” *Acta Mater.* **265**, 119595 (2024).
- Z. Y. Wei, E. K. Liu, Y. Li, X. L. Han, Z. W. Du, H. Z. Luo, G. D. Liu, X. K. Xi, H. W. Zhang, W. H. Wang, and G. H. Wu, “Magnetostructural martensitic transformations with large volume changes and magneto-strains in all-*d*-metal Heusler alloys,” *Appl. Phys. Lett.* **109**, 071904 (2016).
- Z. Q. Guan, J. Bai, Y. Zhang, J. L. Gu, X. Z. Liang, Y. D. Zhang, L. D. Esling, X. Zhao, and L. Zuo, “Simultaneously realized large low-temperature magnetocaloric effect and good mechanical properties in  $Ni_{36}Co_{13}Mn_{35}Ti_{16}$  alloy,” *J. Appl. Phys.* **131**, 165107 (2022).
- D. Y. Cong, W. X. Xiong, A. Planes, Y. Ren, L. Mañosa, P. Y. Cao, Z. H. Nie, X. M. Sun, Z. Yang, X. F. Hong, and Y. D. Wang, “Colossal elastocaloric effect in ferroelastic Ni-Mn-Ti alloys,” *Phys. Rev. Lett.* **122**, 255703 (2019).
- A. Aznar, A. Gràcia-Condal, A. Planes, P. Lloveras, M. Barrio, J. L. Tamarit, W. X. Xiong, D. Y. Cong, C. Popescu, and L. Mañosa, “Giant barocaloric effect in all-*d*-metal Heusler shape memory alloys,” *Phys. Rev. Mater.* **3**, 044406 (2019).
- S. H. Li, D. Y. Cong, W. X. Xiong, Z. Chen, X. Zhang, Z. H. Nie, S. W. Li, R. G. Li, Y. K. Wang, Y. X. Cao, Y. Ren, and Y. D. Wang, “A low-cost Ni-Mn-Ti-B high-temperature shape memory alloy with extraordinary functional properties,” *ACS Appl. Mater. Interfaces* **13**, 31870 (2021).
- S. Samanta, S. Ghosh, and K. Mandal, “Observation of giant exchange bias effect in Ni-Mn-Ti all-*d*-metal Heusler alloy,” *J. Phys.: Condens. Matter* **34**, 105801 (2022).
- S. Samanta, S. Chatterjee, J. Sinha, and K. Mandal, “Giant reversibility of magneto-responsive properties in all-*d*-metal Ni-Co-Mn(Cu)-Ti Heusler alloys: Role of phase-fraction-assisted magnetostructural transition,” *Phys. Rev. Mater.* **7**, 084406 (2023).
- S. W. Li, L. H. He, H. L. Lu, J. Z. Hao, D. K. Wang, F. R. Shen, C. Song, G. J. Liu, P. F. Du, Y. D. Wang, and D. Y. Cong, “Ultra-high-performance solid-solid phase change material for efficient, high-temperature thermal energy storage,” *Acta Mater.* **249**, 118852 (2023).
- V. Chaudhary, Z. Wang, A. Ray, I. Sridhar, and R. V. Ramanujan, “Self pumping magnetic cooling,” *J. Phys. D: Appl. Phys.* **50**, 03LT03 (2017).
- D. J. Silva, B. D. Bordalo, A. M. Pereira, J. Ventura, and J. P. Araújo, “Solid state magnetic refrigerator,” *Appl. Energy* **93**, 570 (2012).
- A. Kitanovski and P. W. Egolf, “Innovative ideas for future research on magnetocaloric technologies,” *Int. J. Refrig.* **33**, 449 (2010).
- S. Pal, A. Datta, S. Sen, A. Mukhopadhyay, K. Bandopadhyay, and R. Ganguly, “Characterization of a ferrofluid-based thermomagnetic pump for microfluidic applications,” *J. Magn. Mater.* **323**, 2701 (2011).
- K. Kliner, M. M. Rojo, Z. Kutnjak, and A. Kitanovski, “Toward a solid-state thermal diode for room-temperature magnetocaloric energy conversion,” *J. Appl. Phys.* **127**, 234101 (2020).

- <sup>29</sup>D. N. Ba, Y. L. Zheng, L. Becerra, M. Marangolo, M. Almanza, and M. LoBue, "Magnetocaloric effect in flexible, free-standing gadolinium thick films for energy conversion applications," *Phys. Rev. Appl.* **15**, 064045 (2021).
- <sup>30</sup>Y. D. Wang, Y. Ren, Z. H. Nie, D. M. Liu, L. Zuo, H. Choo, H. Li, P. K. Liaw, J. Q. Yan, R. J. McQueeney, J. W. Richardson, and A. Huq, "Structural transition of ferromagnetic Ni<sub>2</sub>MnGa nanoparticles," *J. Appl. Phys.* **101**, 063530 (2007).
- <sup>31</sup>X. L. Liu, Y. F. Zhang, Y. Y. Wang, W. J. Zhu, G. L. Li, X. W. Ma, Y. H. Zhang, S. Z. Chen, S. Tiwari, K. J. Shi, S. W. Zhang, H. M. Fan, Y. X. Zhao, and X. J. Liang, "Comprehensive understanding of magnetic hyperthermia for improving antitumor therapeutic efficacy," *Theranostics* **10**, 3793 (2020).
- <sup>32</sup>J. B. Li, Y. Qu, J. Ren, W. Z. Yuan, and D. L. Shi, "Magnetocaloric effect in magnetothermally-responsive nanocarriers for hyperthermia-triggered drug release," *Nanotechnology* **23**, 505706 (2012).
- <sup>33</sup>G. Cavazzini, F. Cugini, D. Delmonte, G. Trevisi, L. Nasi, S. Ener, D. Koch, L. Righi, M. Solzi, O. Gutfleisch, and F. Albertini, "Multifunctional Ni-Mn-Ga and Ni-Mn-Cu-Ga Heusler particles towards the nanoscale by ball-milling technique," *J. Alloys Compd.* **872**, 159747 (2021).
- <sup>34</sup>V. Sánchez-Alarcos, V. Recarte, J. I. Pérez-Landazábal, S. Larumbe, R. Caballero-Flores, I. Unzueta, J. A. García, F. Plazaola, and J. A. Rodríguez-Velamazán, "Mechanically induced disorder and crystallization process in Ni-Mn-In ball-milled alloys," *J. Alloys Compd.* **689**, 983 (2016).
- <sup>35</sup>A. Aslami, M. Ghahremani, M. Zhang, L. H. Bennett, and E. Della Torre, "Enhanced magnetic properties of Ni<sub>51</sub>Mn<sub>33.4</sub>In<sub>15.6</sub> Heusler alloy nanoparticles," *IEEE Trans. Magn.* **53**, 2504006 (2017).
- <sup>36</sup>F. Q. Zhang, C. Taake, B. W. Huang, X. M. You, H. Ojjiyed, Q. Shen, I. Dugulan, L. Caron, N. van Dijk, and E. Brück, "Magnetocaloric effect in the (Mn,Fe)<sub>2</sub>(P,Si) system: From bulk to nano," *Acta Mater.* **224**, 117532 (2022).
- <sup>37</sup>M. R. Karim, S. N. Panda, A. Barman, and I. Sarkar, "Strain and crystallite size controlled ordering of Heusler nanoparticles having high heating rate for magneto-thermal application," *Nanotechnology* **33**, 235701 (2022).
- <sup>38</sup>Y. L. Xu, L. Liu, G. D. Lu, L. Z. Yi, M. Liu, H. G. Piao, and L. Q. Pan, "Dynamic magnetic properties of Ni<sub>2</sub>FeGa Heusler alloy nanoparticles," *J. Nanopart. Res.* **23**, 123 (2021).
- <sup>39</sup>R. Ghunaim, V. Eckert, M. Scholz, M. Gellesch, S. Wurmehl, C. Damm, B. Büchner, M. Mertig, and S. Hampel, "Carbon nanotube-assisted synthesis of ferromagnetic Heusler nanoparticles of Fe<sub>3</sub>Ga (Nano-Galfenol)," *J. Mater. Chem. C* **6**, 1255 (2018).
- <sup>40</sup>A. Ahmad, S. Mitra, S. K. Srivastava, and A. K. Das, "Giant magnetocaloric effect in Co<sub>2</sub>FeAl Heusler alloy nanoparticles," *J. Phys. D: Appl. Phys.* **54**, 385001 (2021).
- <sup>41</sup>C. H. Wang, Y. Z. Guo, F. Casper, B. Balke, G. H. Fecher, C. Felser, and Y. Hwu, "Size correlated long and short range order of ternary Co<sub>2</sub>FeGa Heusler nanoparticles," *Appl. Phys. Lett.* **97**, 103106 (2010).
- <sup>42</sup>C. H. Wang, L. Basit, Y. Khalavka, Y. Z. Guo, F. Casper, T. Gasi, V. Ksenofontov, B. Balke, G. H. Fecher, C. Sönnichsen, Y. K. Hwu, J. J. Lee, and C. Felser, "Probing the size effect of Co<sub>2</sub>FeGa-SiO<sub>2</sub>@C nanocomposite particles prepared by a chemical approach," *Chem. Mater.* **22**, 6575 (2010).
- <sup>43</sup>C. H. Wang, "A chemical approach to Heusler compounds and nanoparticles," Ph.D. thesis (Johannes Gutenberg-Universität Mainz, 2011).
- <sup>44</sup>C. H. Wang, A. A. Levin, L. Nasi, S. Fabbri, J. Qian, C. E. V. Barbosa, S. Ouardi, J. Karel, F. Albertini, H. Borrmann, G. H. Fecher, and C. Felser, "Chemical synthesis and characterization of  $\gamma$ -Co<sub>2</sub>NiGa nanoparticles with a very high Curie temperature," *Chem. Mater.* **27**, 6994 (2015).
- <sup>45</sup>J. C. Feng, R. Geutjens, N. V. Thang, J. J. Li, X. A. Guo, A. Keri, S. Basak, G. Galbacs, G. Biskos, H. Nirschl, H. W. Zandbergen, E. Brück, and A. Schmidt-Ott, "Magnetic phase transition in spark-produced ternary LaFeSi nanoalloys," *ACS Appl. Mater. Interfaces* **10**, 6073 (2018).
- <sup>46</sup>J. C. Feng, "Scalable spark ablation synthesis of nanoparticles: Fundamental considerations and application in textile nanofinishing," Ph.D. thesis (Delft University of Technology, 2016).
- <sup>47</sup>A. Schmidt-Ott, *Spark Ablation: Building Blocks for Nanotechnology* (CRC Press, 2019).
- <sup>48</sup>I. Nkurikiyimfura, Y. M. Wang, and Z. D. Pan, "Heat transfer enhancement by magnetic nanofluids: A review," *Renewable Sustainable Energy Rev.* **21**, 548 (2013).
- <sup>49</sup>M. Kole and S. Khandekar, "Engineering applications of ferrofluids: A review," *J. Magn. Magn. Mater.* **537**, 168222 (2021).
- <sup>50</sup>T. W. Jin and Y. S. Jung, "Classifying intermetallic tetragonal phase of all-d-metal Heusler alloys for catalysis applications," *Top. Catal.* **65**, 208 (2022).
- <sup>51</sup>J. M. D. Coey, *Magnetism and Magnetic Materials* (Cambridge University Press, 2010).
- <sup>52</sup>A. H. Lu, E. L. Salabas, and F. Schuth, "Magnetic nanoparticles: Synthesis, protection, functionalization, and application," *Angew. Chem. Int. Ed.* **46**, 1222 (2007).
- <sup>53</sup>R. Sappey, E. Vincent, N. Hadacek, F. Chaput, J. P. Boilot, and D. Zins, "Nonmonotonic field dependence of the zero-field cooled magnetization peak in some systems of magnetic nanoparticles," *Phys. Rev. B* **56**, 14551 (1997).
- <sup>54</sup>M. Jeddi, H. Gharsallah, M. Bekri, E. Dhahri, and E. K. Hlil, "Structural characterization and ZFC/FC magnetization study of La<sub>0.6</sub>Ca<sub>0.4-x</sub>Sr<sub>x</sub>MnO<sub>3</sub> nanoparticle compounds," *Appl. Phys. A* **126**, 6 (2020).
- <sup>55</sup>F. Q. Zhang, J. J. Fang, L. Huang, W. M. Sun, Z. Q. Shi, X. W. Kang, and S. W. Chen, "Alkyne-functionalized ruthenium nanoparticles: Impact of metal-ligand interfacial bonding interactions on the selective hydrogenation of styrene," *ACS Catal.* **9**, 98 (2019).
- <sup>56</sup>W. Zhang, "Nanoparticle aggregation: Principles and modeling," in *Nanomaterial: Impacts on Cell Biology Medicine* (Springer Science & Business Media, 2014), p. 19.
- <sup>57</sup>X. W. Zhou, R. A. Johnson, and H. N. G. Wadley, "Misfit-energy-increasing dislocations in vapor-deposited CoFe/NiFe multilayers," *Phys. Rev. B* **69**, 144113 (2004).
- <sup>58</sup>R. Vishnoi, R. Singhal, and D. Kaur, "Thickness dependent phase transformation of magnetron-sputtered Ni-Mn-Sn ferromagnetic shape memory alloy thin films," *J. Nanopart. Res.* **13**, 3975 (2011).
- <sup>59</sup>P. Ranzieri, S. Fabbri, L. Nasi, L. Righi, F. Casoli, V. A. Chernenko, E. Villa, and F. Albertini, "Epitaxial Ni-Mn-Ga/MgO(100) thin films ranging in thickness from 10 to 100 nm," *Acta Mater.* **61**, 263 (2013).
- <sup>60</sup>T. Waitz, V. Kazykhanov, and H. P. Karnthaler, "Martensitic phase transformations in nanocrystalline NiTi studied by TEM," *Acta Mater.* **52**, 137 (2004).
- <sup>61</sup>C. H. Wang, J. Meyer, N. Teichert, A. Auge, E. Rausch, B. Balke, A. Hütten, G. H. Fecher, and C. Felser, "Heusler nanoparticles for spintronics and ferromagnetic shape memory alloys," *J. Vac. Sci. Technol. B* **32**, 020802 (2014).
- <sup>62</sup>K. H. J. Buschow, *Handbook of Magnetic Materials* (Elsevier, 2015), Vol. 23.
- <sup>63</sup>S. Yoon, "Determination of the temperature dependence of the magnetic anisotropy constant in magnetite nanoparticles," *J. Korean Phys. Soc.* **59**, 3069 (2011).
- <sup>64</sup>F. Fabris, J. Lohr, E. Lima, A. A. De Almeida, H. E. Troiani, L. M. Rodríguez, M. V. Mansilla, M. H. Aguirre, G. F. Goya, and D. Rinaldi, "Adjusting the Néel relaxation time of Fe<sub>3</sub>O<sub>4</sub>/Zn<sub>x</sub>Co<sub>1-x</sub>Fe<sub>2</sub>O<sub>4</sub> core/shell nanoparticles for optimal heat generation in magnetic hyperthermia," *Nanotechnology* **32**, 065703 (2020).
- <sup>65</sup>C. Antoniak, J. Lindner, and M. Farle, "Magnetic anisotropy and its temperature dependence in iron-rich Fe<sub>x</sub>Pt<sub>1-x</sub> nanoparticles," *Europhys. Lett.* **70**, 250 (2005).
- <sup>66</sup>S. Yoon and K. M. Krishnan, "Temperature dependence of magnetic anisotropy constant in manganese ferrite nanoparticles at low temperature," *J. Appl. Phys.* **109**, 07B534 (2011).
- <sup>67</sup>V. V. Warhate and D. S. Badwaik, "Structural, magnetic and thermo-magnetic properties of NiMn Y-Type strontium nano-hexaferrites," *J. Alloys Compd.* **818**, 152830 (2020).
- <sup>68</sup>A. M. Abdallah, A. Aridi, M. Rabaa, R. M. Moussa, and R. Awad, "Tailored physical and magnetic properties by La<sup>3+</sup> dopants in Mg-Ni-Co nanoferrites: Insight into the law of approach to saturation," *Appl. Phys. A* **129**, 770 (2023).
- <sup>69</sup>B. D. Cullity and C. D. Graham, *Introduction to Magnetic Materials*, 2nd ed. (John Wiley & Sons, 2009).